(31) Statman, D.; Chu, B. *Macromolecules* **1984**, *17*, 1537.
(32) Riseman, J.; Kirkwood, J. G. *J. Chem. Phys.* **1950**, *18*, 512. Kirkwood, J. G.; Auer, P. L. *Ibid* **1951**, *19*, 281.
(33) Ambler, M.; McIntyre, D.; Fetters, L. J. *Macromolecules* **1978**, *11*, 300.
(34) Berger, M.; Tidswell, B. M. *J. Polym. Sci., Polym. Symp.* **1973**, *42*, 1063.
(35) Broersma, S. *J. Chem. Phys.* **1960**, *32*, 1626, 1632; **1981**, *74*, 6989.
(36) Lewis, R. J. Ph.D. Thesis, Stanford University, 1985.
(37) Russo, P. S.; Miller, W. G. *Macromolecules* **1984**, *17*, 1324.
(38) Bersted, B. *J. Appl. Polym. Sci.* **1973**, *17*, 1415.
(39) Marrucci, G.; Grizzuti, N. *J. Polym. Sci., Polym. Lett. Ed.* **1983**, *21*, 83.
(40) Maier, K. R. Ph.D. Thesis, Stanford University, 1986.
(41) Provencher, S.; Hendrix, J.; DeMayer, L. *J. Chem. Phys.* **1978**, *69*, 4273. Provencher, S. *Makromol. Chem.* **1979**, *180*, 201; *Comput. Phys. Commun.* **1982**, *27*, 213, 229.
(42) Bott, S. E. In *Measurement of Suspended Particles by Quasi-Elastic Light Scattering*; Dahneke, B., Ed.; Wiley: New York, 1983; Ph.D. Thesis, Stanford University, 1984.
(43) Malmberg, M. S.; Lippincott, E. R. *J. Colloid Interface Sci.* **1968**, *27*, 591. Huglin, M. B., Ed. *Light Scattering from Polymer Solutions*; Academic: London, England, 1972.
(44) Russo, P. S.; Langley, K.; Karasz, F. E. *J. Chem. Phys.* **1984**, *80*, 5312.
(45) Jamieson, A.; Southwick, J.; Blackwell, J. *J. Polym. Sci., Polym. Phys. Ed.* **1982**, *20*, 1513.
(46) Zero, K. M.; Pecora, R. *Macromolecules* **1982**, *15*, 87.
(47) Aharoni, S. M.; Walsh, E. K. *Macromolecules* **1979**, *12*, 271. Aharoni, S. M. *J. Polym. Sci., Polym. Phys. Ed.* **1980**, *18*, 1303, 1439.
(48) Kubota, K.; Chu, B. *Biopolymers* **1983**, *22*, 1461.
(49) Kubota, K.; Chu, B. *Macromolecules* **1983**, *16*, 105.
(50) Pecora, R. *J. Chem. Phys.* **1968**, *48*, 4126; **1968**, *49*, 1032.
(51) Pusey, P. N.; Fijnaut, H. M.; Vrij, A. *J. Chem. Phys.* **1982**, *77*, 4270.
(52) Lee, W. I.; Schmitz, K. S.; Lin, S.-C.; Schurr, J. M. *Biopolymers* **1977**, *16*, 583.
(53) Hartl, W.; Versmold, H. *J. Chem. Phys.* **1984**, *80*, 1387.
(54) Han, C. C.; Schaefer, D. W. In *Dynamic Light Scattering: Applications of Photon Correlation Spectroscopy*; Pecora, R., Ed.; Plenum: New York, 1985.
(55) Brown, W. *Macromolecules* **1984**, *17*, 66.
(56) Balloge, S.; Tirrell, M. *Macromolecules* **1985**, *18*, 817.
(57) Aragon, S. R.; Pecora, R. *J. Chem. Phys.* **1985**, *82*, 5346.

Phase Separation in Ternary Systems Solvent–Polymer 1–Polymer 2. 3. Homogeneous Double Critical Points

K. Šolc* and Y. C. Yang

Michigan Molecular Institute, Midland, Michigan 48640. *Received June 2, 1987*

ABSTRACT: A number of quantitative relations have been developed for homogeneous double critical points (HODCP's) in Flory–Huggins ternary systems solvent–polymer 1–polymer 2 with interactions characterized by polymer–polymer parameter g_x and solvent–polymer parameters g_1 and g_2. Their location in the composition diagram is restricted to three linear segments, and they can exist only for combinations of g_x and Δg ($\Delta g \equiv g_2 - g_1$) limited to double-sector areas of the $g_x,\Delta g$ plane. The lower sectors contain exclusively *elliptic* HODCP's marking disappearance of closed-loop binodals, while the upper sectors are divided between *hyperbolic* (marking confluence of two binodal regions) and *unstable elliptic* types. Sector vertices represent unique systems where the effect of unequal chain lengths is just balanced by interactions to produce a constant critical temperature, independent of composition. Conditions for multiple occurrence of HODCP's and relations for orientation of spinodals at HODCP's are derived. Special attention is paid to systems located on hyperbolic boundaries between elliptic and hyperbolic regions where HODCP's overlap with heterogeneous double critical points. A criterion is also given for improving the solvent power in terms of interaction parameter perturbations.

1. Introduction

Homogeneous double critical points (HODCP's) in ternary systems mark conspicuous changes in the pattern of isothermal spinodals and binodals. In one instance (which might be called *elliptic*) it is the disappearance from the phase diagram of loop-shaped binodals that defines closed, usually two-phase regions (sequence T_3, T_2, T_1, T_0 in Figure 1); in the other case (*hyperbolic*), two regular growing two-phase regions coalesce into a single two-phase region without a critical point (sequence T_2, T_1, T_0, T_{-1} in Figure 2). In both instances two real single critical points of the same kind approach each other with changing temperature, merge into a HODCP at T_0, and become complex (i.e., disappear from the real space).[1,2]

So far the occurrence of HODCP's has been studied only for two simple extreme cases: (i) they were detected in regular ternary solutions whose components differ in interactions but not in molecular volumes;[3] (ii) it has also been shown that they *cannot* exist in quasi-binary solutions whose polymeric components differ but by their chain lengths.[4] Thus some degree of disparity in interactions between the three components seems necessary for their appearance. On the other hand, the chain-length effect, although by itself incapable of producing the HODCP's, will certainly modify their location in the space of variables if combined with the difference in interactions. In order to gain quantitative knowledge about the interplay of these two factors, the conditions are here examined for the existence of HODCP's in general Flory–Huggins ternary systems solvent (0)–polymer (1)–polymer (2). A preliminary report on this subject was given in ref 5.

2. Critical State Conditions

The critical state in the examined system is defined by the following three functions:[2,6]

$$F_c \equiv \Phi^2\langle r\xi\rangle^3 - \langle r^2\xi^3\rangle = 0 \tag{1}$$

$$G_c \equiv \xi^2(1 - \varphi_2 r_2 P) - (1 - \varphi_1 r_1 M) = 0 \tag{2}$$

$$H_c \equiv \xi^2 + 1 + \varphi\{\xi\langle r\xi\rangle[(2/\varphi_0) - 4\bar{g}] + w_1 r_1 P + \xi^2 w_2 r_2 M\} = 0 \tag{3}$$

where φ_i is the volume fraction of the component i, with φ being the total volume fraction of the polymeric solute, $\varphi = \varphi_1 + \varphi_2$; Φ stands for the ratio $\Phi = \varphi/\varphi_0$; the construct $\langle\ \rangle$ denotes the moment

$$\langle r^i\xi^j\rangle = w_1 r_1{}^i\xi^{-j} + w_2 r_2{}^i\xi^j$$

where $w_m = \varphi_m/\varphi$, $m = 1, 2$, are the volume fractions of

0024-9297/88/2221-0829$01.50/0

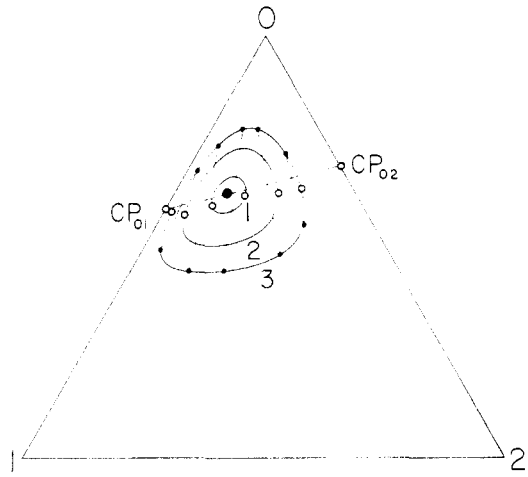

Figure 1. Schematic sketch of several binodals for temperatures T_1, T_2, and T_3 around an *elliptic* homogeneous double critical point (●) at T_0. (○) Single critical points; CP_{ij}, binary critical point for the mixture of components i and j; (●—●) tie-lines for the binodal T_3.

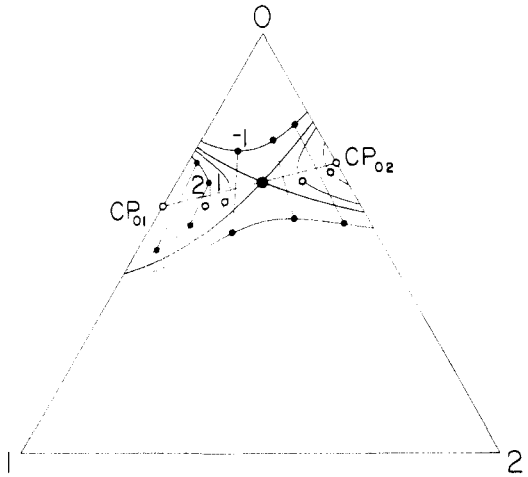

Figure 2. Schematic sketch of several binodals for temperatures T_{-1}, T_0, T_1, and T_2 around a *hyperbolic* homogeneous double critical point (●) at T_0. Symbol definitions are the same as in Figure 1, only the tie lines are drawn for parts of binodals T_2 and T_{-1}.

polymers 1 and 2 in their mixture, ξ^2 is the critical ratio of Flory's separation factors

$$\xi^2 \equiv \lim_{\sigma_m \to 0} \sigma_2/\sigma_1 \tag{4}$$

and r_m is the relative chain length of the polymer m where $1 \leq r_1 \leq r_2$. The mean Flory–Huggins polymer–solvent interaction parameter is defined as $\bar{g} = (g_1 + g_2)/2$, and P and M stand for the sum and the difference, respectively, between the polymer–polymer interaction parameter g_x and the difference of the two solvent parameters $\Delta g \equiv g_2 - g_1$, i.e., $P \equiv g_x + \Delta g$ and $M \equiv g_x - \Delta g$. All interaction parameters are in principle functions of temperature, but they are assumed to be independent of the system composition.

3. Homogeneous Double Critical Points

As shown recently by two independent methods,[2] the condition for a HODCP is very simple if expressed in terms of the parameter ξ^2: it is required that ξ^2 assumes one of only two values

$$\xi^2 = \pm\rho_1/\rho_2 \tag{5}$$

where $\rho_m = r_m^{1/2}$. It then follows from the F_c function (eq 1) that the position of HODCP's within the composition triangle is severely restricted: they can be located only on one of the three linear segments connecting the binary critical points (see Figure 3). Specifically, for positive ξ^2 the critical concentration is given by

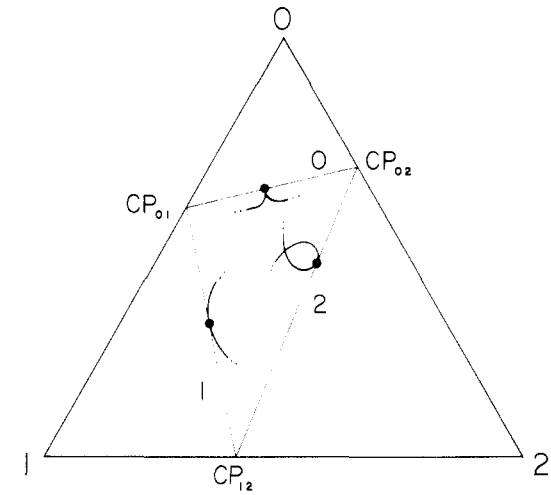

Figure 3. Linear segments 0, 1, and 2 in the triangle of composition, representing loci of homogeneous double critical points (HODCP) with positive (0) and negative (1, 2) ξ^2 of eq 5, respectively. CP_{ij}, binary critical points; CP_{12} marks the Scott composition w_2^S (eq 12); (–●–) three examples of HODCP's with different shapes of critical lines.

$$\varphi = (1 + w_1\rho_1 + w_2\rho_2)^{-1} \tag{6}$$

placing the HODCP on the segment 0 joining the two solvent–polymer critical points CP_{01} and CP_{02} (as also seen in Figures 1 and 2), whereas for a negative ξ^2 the HODCP is located on one of the two linear segments, 1 or 2, originating in the binary critical point CP_{12} for the mixture of the polymers 1 and 2, with the concentration given as

$$\varphi = (1 + |w_1\rho_1 - w_2\rho_2|)^{-1} \tag{7}$$

This segment notation differs from the one used previously[6] but is perhaps more logical: it is tied to the apex whose region the given segment spans.

A deeper insight into the origins of the HODCP multiplicity is provided by our recently developed novel approach to identifying multiple critical points.[2,6] Their double nature is due to the double-rootiness of the critical quantity ξ^2 in eq 1. Viewed as a cubic equation for the unknown ξ^2, this relation can be solved and the resulting ξ^2 plotted as a surface above the composition triangle φ, w. Since a cubic equation can have one or three real different roots, the ξ^2 surface is expected to be quite complicated. Indeed, it has three single-valued apex portions, each associated with one triangle apex and smoothly continuing into the common central region where all of them overlap, forming a three-valued surface (see Figures 5 and 6 of ref 6). It is apparent that double roots of ξ^2 can exist only at the boundaries of the three-valued region where always two different portions of the surface are fused together (e.g., surfaces 1 and 2 are joined at the boundary 0), and the tangential planes become vertical. The three boundaries of the multivalued region for ξ^2 are of course identical with the linear loci of HODCP's defined by eq 6 and 7 and displayed in Figure 3. The critical line $\xi^2(w_2)$ of a given system,[7] embedded in the ξ^2 surface, swings at a HODCP from one surface portion to another; hence its projection in Figures 1–3 has to contact the corresponding linear segment from the *inside*. This behavior is in stark contrast to that of *heterogeneous* double critical points whose multiplicity originates in the cloud-point equation rather than in the critical formula 1; such points do not

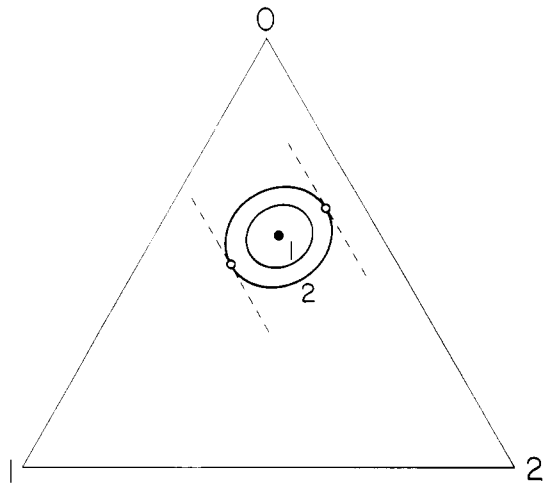

Figure 4. (●) Spinodals for a system with an elliptic HODCP. (○) Points of contact between the spinodal 2 and the lines of constant φ_1 (- - -).

require double roots of ξ^2 and can be located in principle anywhere in the composition triangle.[2]

While the criterion (5) is very simple, without further analysis it is not too helpful in estimating the phase behavior of any particular system characterized in terms of the interaction parameters $g(T)$, since the relation between the two via eq 1–3 is not trivial. Below we address this problem by interpreting the above result in terms of common physical variables such as interaction parameters, polymer composition, etc. and by answering a host of interesting practical questions. The first one might be: Can one predict whether a HODCP will be of elliptic or hyperbolic type, so different in their consequences for the phase behavior?

3.1. Distinction between Elliptic and Hyperbolic Types. The two types of HODCP's can be distinguished, e.g., by their spinodals that follow patterns similar to those of binodals displayed in Figures 1 and 2. One can utilize the fact that only in the elliptic case the spinodal unconditionally changes from real to complex (i.e., disappears from the real space) when crossing the HODCP temperature, while in the hyperbolic case it changes its pattern but stays real at least in part of the composition interval.

The spinodal is quadratic in volume fractions φ_1 and φ_2;[8] for instance, it can be written as

$$A\varphi_2^2 + B\varphi_2 + C = 0 \tag{8}$$

where the coefficients are functions of φ_1 and T. Since the sought distinction has to do with real and complex solutions, the feature to be examined is the behavior around zero of the discriminant $D \equiv B^2 - 4AC$. It is apparent that for a chosen temperature, the condition $D = 0$ fixes the value(s) of φ_1 whereas relative to the variable φ_2 of eq 8 it specifies its double root. Physically, $D = 0$ thus defines point(s) of contact between the respective spinodal and line(s) of constant φ_1, as shown in Figure 4.

A HODCP is characterized by merging of two such contact points into a single one, mathematically reflected by the additional condition $(\partial D/\partial\varphi_1)_T = 0$. The function $D(\varphi_1)$ thus has to display an extremum touching on the $D = 0$ axis. Specifically, an elliptic HODCP will be characterized by a *maximum* since a temperature perturbation in the right direction has to bring the contact-point neighborhood of the $D(\varphi_1)$ function into a negative half-plane, making the spinodals complex. On the other hand the hyperbolic type will correspond to a *minimum*, leaving even after perturbation the spinodal real at least in part of the φ_1 interval. The decisive factor thus turns out to be the sign of the second composition derivative of the discriminant, $D'' \equiv (\partial^2 D/\partial\varphi_1^2)_T$, with the negative sign indicating an elliptic type and a positive sign denoting a hyperbolic type. The general form for D'' is rather unattractive

$$D'' = 3(Z - 2\phi_1 r_1 r_2 Q)^2 - Z^2 - 4r_1 r_2[8r_1 g_1 g_x + Q(1 - 2r_1 - r_2(2g_2 - 1))] \tag{9}$$

where

$$Z = 2(r_2 g_2 - r_1 g_1 - r_1 r_2 g_x) + r_1 r_2 Q$$

$$Q = 4g_1 g_2 - (g_1 + g_2 - g_x)^2$$

However, this expression (as well as others) can be greatly simplified when considered separately for each of the three linear segments where the HODCP's have to be located. The triplet of results thus obtained possesses a high degree of symmetry, allowing them to be expressed in terms of universal functions whose parameters assume different meanings for different linear segments, as demonstrated below.

3.2. Critical Point Diagrams. Critical point diagrams display ranges of existence of various critical points. They do not relate to any particular system; rather they are of global nature, displaying all critical points of the examined type that can exist in various systems of the given class. Examples of such diagrams have been reported in ref 9, Figures 4, 6, and 7, for binary systems with concentration-dependent parameter g, and in ref 10, Figure 2, for quaternary quasi-binary systems. Here the concept of critical diagrams is extended to the HODCP's in ternary systems.

HODCP's have to satisfy four relations, e.g., eq 1–3 and 5; this allows elimination of four out of six $(\xi^2,\varphi,w_2,\bar{g},\Delta g,g_x)$ variables, leaving just two of them as independent. Perhaps the most convenient choice for the latter two are the variables g_x and Δg expressing the deviations from the quasi-binary reference system.

For a HODCP located on the "solvent" segment 0 (case 0) the relation for w_2 calculated from eq 2, 5, and 6 is

$$w_2 = \frac{r_1\rho_2 M - (\rho_2 - \rho_1)(1 + \rho_1)}{\rho_1\rho_2(\rho_1 M + \rho_2 P) + (\rho_2 - \rho_1)^2} \tag{10}$$

The requirement that $0 \le w_2 \le 1$ then imposes bounds through eq 10 on the definition range of HODCP's in the $g_x,\Delta g$ space: they are restricted to two 90° sector-shaped areas symmetrically positioned about an off-origin vertex V_0 as shown in Figure 5. The structure of this graph is surprisingly simple; e.g., loci of HODCP's with a given polymer composition w_2 (and a given φ) are linear, with slopes

$$\mathrm{d}g_x/\mathrm{d}\Delta g = (w_1\rho_1 + w_2\rho_2)/(w_1\rho_1 - w_2\rho_2) \tag{11}$$

The iso-w_2 lines thus fan across the entire double sector, starting from the bound a with the composition $w_{2,a} = 0$ and angle $\omega_a = 45°$ and ending at the bound b of composition $w_{2,b} = 1$ and angle $\omega_b = 135°$. The line corresponding to the Scott composition[6,11]

$$w_2^{\mathrm{S}} = \rho_1/(\rho_1 + \rho_2) \tag{12}$$

is vertical. These statements are summarized on the first line of Table I.

Analogous relations for HODCP's situated on the "polymer" segments 1 and 2 are recovered from the original segment-0 formulas 10 and 11 by modifying the signs of one of the ρ terms as indicated in columns 7 and 8 of Table I. For instance for a HODCP residing on the linear segment 1 (case 1), the equations are modified by switching the sign of ρ_2, with angles of iso-w_2 lines now varying from

Table I
Some Characteristics of Homogeneous Double Critical Points

	definition interval[b]					transformation rules			
case[a]	$w_{2,a}$	ω_a	$w_{2,b}$	ω_b	w_2^S			X	Y
0	0	$\pi/4$	1	$3\pi/4$	v	ρ_1	ρ_2	ν	μ
1	w_2^S	0	0	$\pi/4$	h	ρ_1	$-\rho_2$	μ	ν
2	1	$3\pi/4$	w_2^S	π	h	$-\rho_1$	ρ_2	$-\mu$	$-\nu$

[a] Identifies the segment where the HODCP is located. [b] The polymer composition w_2 and the angle ω of the sector bounds a and b. At the Scott composition w_2^S, v and h stand for vertical and horizontal, respectively.

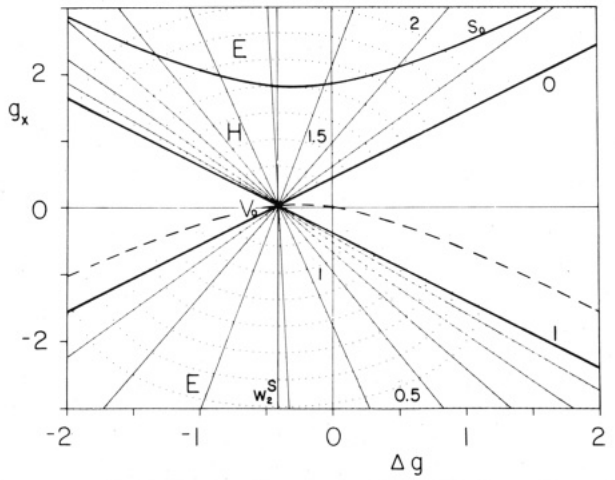

Figure 5. Critical point diagram for HODCP's located on the solvent segment 0 for a system with $r_1 = 2$, $r_2 = 5$. (—) Straight lines of constant composition w_2 incremented by 0.1, with an additional vertical for $w_2 = w_2^S$; 0 and 1 stand for compositions at the interval bounds. (···) Circular loci of constant $\bar{g}$ (here distorted into ellipses) incremented by 0.1, with some $\bar{g}$ values indicated. V_0, sector vertex; s_0, hyperbolic boundary between hyperbolic (H) and elliptic (E) regions, with dashed line indicating its physically insignificant branch.

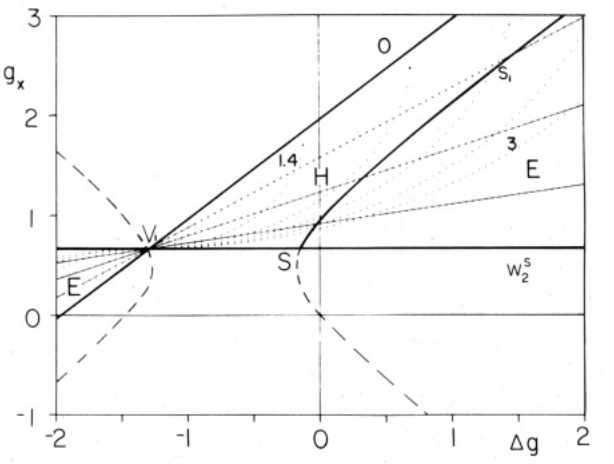

Figure 6. Critical point diagram for HODCP's located on the segment 1. The system and the notation are the same as in Figure 5 except for the increments in iso-$\bar{g}$ lines (···) that are 0.4.

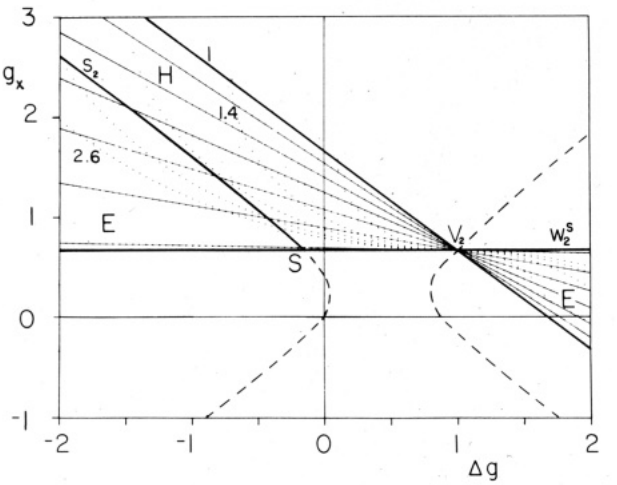

Figure 7. Critical point diagram for HODCP's located on the segment 2. The system and notation are the same as in Figure 6.

zero for Scott composition to 45° for $w_2 = 0$ (Figure 6). On the other hand, the segment-2 HODCP's are characterized by lines spreading from 135° for $w_2 = 1$ to 180° for Scott's line and by relations for w_2 and the slope obtained from eq 10 and 11 by changing the sign of ρ_1 (Figure 7). Note that the transformation rules for ρ_m are also applicable to relations for ξ^2 and φ, eq 5 and 6, where they switch the sign and produce eq 7, respectively.

At the vertex V the composition w_2 should be undefined, hence the vertex coordinates Δg^v and $g_x{}^v$ can be determined by putting both the numerator and denominator of eq 10 equal to zero. The result is best written in terms of quantities X and Y

$$\Delta g^v = -2Y(1 + X) \qquad g_x{}^v = 2Y^2 \tag{13}$$

whose definitions for various cases are given in the last two columns of Table I. For instance for the case 0 (Figure 5), $X = \nu$ and $Y = \mu$ where

$$\nu = (\rho_2 + \rho_1)/2\rho_1\rho_2 \qquad \mu = (\rho_2 - \rho_1)/2\rho_1\rho_2 \tag{14}$$

for the case 1 (Figure 6), $X = \mu$ and $Y = \nu$, etc. From eq 14 it is apparent that, again, the transformation rules for X and Y are consistent with the rules for ρ_1 and ρ_2.

The mean value of the solvent interaction parameter $\bar{g}$ required for the appearance of a HODCP is now given from eq 3 simply as

$$4\bar{g} = 4\bar{g}^v + (g_x - g_x{}^v) + \frac{[\Delta g - \Delta g^v]^2}{(g_x - g_x{}^v)} \tag{15a}$$

where its vertex value is

$$\bar{g}^v = [Y^2 + (1 + X)^2]/2 \tag{15b}$$

The vertex of each sector-shaped definition range thus turns out to be an important point: in relative coordinates referred to it, $g^\dagger \equiv g - g^v$, the mean solvent interaction parameter $\bar{g}^\dagger$ at a HODCP becomes a universal function of "relative heterointeractions"

$$4\bar{g}^\dagger g_x{}^\dagger = g_x{}^{\dagger 2} + (\Delta g^\dagger)^2 \tag{15c}$$

independent of chain lengths r_1 and r_2, as well as independent of which linear segment the HODCP occupies. (Both of these factors, however, do affect the *position* of the vertices as apparent from Figures 5–7, and eq 13 and 15b.)

Equation 15c reveals that lines of constant $\bar{g}^\dagger$ are incomplete circles of the radius

$$R = |2\bar{g}^\dagger| \tag{16a}$$

whose centers in Figures 5–7 are projected above or below

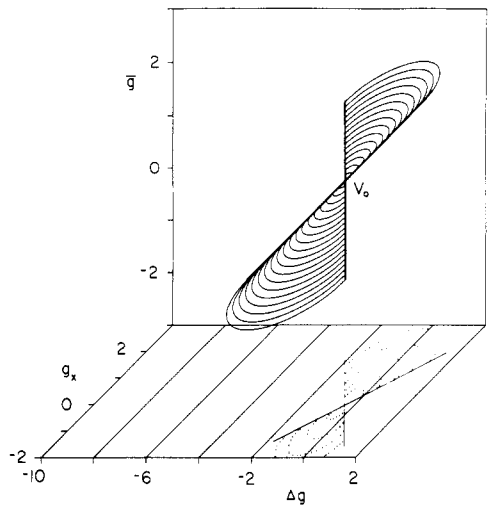

Figure 8. Three-dimensional view of the locus of HODCP's (i.e., the $\bar{g}$ surface) for case 0, in the space of absolute interaction parameters g_x, Δg, and $\bar{g}$ for a system with $r_1 = 2$, $r_2 = 5$. (▬) Bounds of the surface; (—) circular lines of constant $\bar{g}$ with increments of 0.05. In the base-plane projection these lines are marked (—) and (···), respectively.

the corresponding sector vertex in such a way that each circle, if completed, would pass through it. The relative coordinates of the circle centers are

$$\Delta g^{c\dagger} = 0 \qquad g_x^{c\dagger} = 2\bar{g}^{\dagger} \tag{16b}$$

In three-dimensional space $g_x,\Delta g,\bar{g}$ the locus of HODCP's is a section of a deformed double-conical surface, such as displayed for the case 0 in Figure 8. Interestingly, thanks to the universality of eq 15c and complementarity of angular definition ranges ω (cf. Table I), the combined plot for all three cases of the $\bar{g}^{\dagger}$ surface in *relative* coordinates would generate a smooth deformed double half-cone; in *absolute* coordinates, however, this surface splits into three separate, mutually shifted sections of 90° for case 0 (Figure 8) and 45° for cases 1 and 2.

Also the unwieldy eq 9 for D'' can be considerably simplified when examined for a specific linear segment; e.g., for the case 0 the condition for the boundaries between elliptic and hyperbolic HODCP's takes the form

$$D'' \equiv -8\rho_1^3\rho_2^3\frac{[Y\Delta g + (X+1)g_x]}{g_x - 2Y^2}\{g_x[g_x - 2(Y^2 + X^2 + X)] - \Delta g[\Delta g + 2Y(1+2X)]\} = 0 \tag{17}$$

In each of the three cases, this expression generates altogether three boundaries with $D'' = 0$ and one singular line where $D'' \to \pm\infty$. Fortunately most of these curves turn out to be unimportant (except for contributing to the change of sign) since they lie outside the HODCP's definition interval.

The simplest zero boundary is the one given by the numerator of the fraction in eq 17 being equal to zero; it is a straight line with the slope

$$g_x/\Delta g = -Y/(X+1) = g_x^{v}/\Delta g^{v} \tag{18}$$

passing through the origin and through the vertex, thus obviously never entering any of the sector regions proper (not indicated in Figures 5–7).

The second and third zero boundaries can be recovered by solving the quadratic equation in the braces of eq 17; they turn out to be two branches of a hyperbola with a center at $g_x^{h},\Delta g^{h}$ where

$$\Delta g^{h} = -Y(1+2X) \qquad g_x^{h} = Y^2 + X(1+X) \tag{19a}$$

The boundary condition becomes simpler when expressed in coordinates relative to the hyperbola center, $g^* \equiv g - g^{h}$; it is then

$$\mathcal{H} \equiv g_x^{*2} - \Delta g^{*2} - (g_x^{h\,2} - \Delta g^{h\,2}) = 0 \tag{19b}$$

however, in contrast to eq 15c, it contains an absolute term sensitive to ρ_m and affecting the eccentricity of the boundary. The hyperbola's focal axis is vertical for case 0 (where $|g_x^{h}| > |\Delta g^{h}|$) and horizontal for cases 1 and 2 (where $|\Delta g^{h}| > |g_x^{h}|$), and the slopes of asymptotes in all cases are ±1 (cf. Figures 5–7).

It is apparent from comparison of eq 13 and 19a that the centers of hyperbolic boundaries do not coincide with vertices of sector-shaped definition ranges for HODCP's, while the ±45° asymptotes stay parallel to the $w_2 = 1$ and $w_2 = 0$ sector bounds. This relative displacement results in one branch of each hyperbola always staying outside the definition range for the respective HODCP's. For instance, in case 0 only the upper branch s_0 is physically meaningful (drawn in full), while the lower branch passing through the origin and the sector vertex is unimportant (dashed in Figure 5). In the remaining instances (Figures 6 and 7) the conditions are even more restrictive since the sectors spread only over 45°: In case 1 less than the upper right quarter of the hyperbola is significant, whereas in case 2 it is less than the upper left quarter. Both curves s_1 and s_2 end in the common point on the Scott-composition horizontal line, specifically at the half-point S between the two vertices, with the coordinates $g_x^{S} = 2\nu^2$ and $\Delta g^{S} = -2\mu\nu$, which satisfy the condition for a Scott system, $(g_x/\Delta g)_S = -\nu/\mu$ (see Ref. 6, eq 29). In both cases the origin is located on the extended portions of the above mentioned curves, whereas the vertex V lies on the other, physically insignificant, branch of the hyperbolas (dashed in Figures 6 and 7).

A very interesting property of the boundary s becomes apparent from two other symmetrical forms of its criterion which can be derived from eq 19b, namely,

$$r_1\varphi_1 M - 1 = 0 \quad \text{and} \quad r_2\varphi_2 P - 1 = 0 \tag{20}$$

In view of eq 6a–6c, ref 2, these relations imply that all elements of the Gibbs spinodal matrix here become zero, and a check of Korteweg's criterion for double heterogeneous critical points (cf. eq 7 of ref 2) reveals that it is trivially satisfied. Thus the boundary s represents a unique situation where homogeneous and heterogeneous double critical points overlap. Moreover, since it is known that heterogeneous double critical points normally stand between (meta)stable and unstable critical points,[1] one can conclude that the thermodynamic stability of the separated hyperbolic and elliptic HODCP's has to be different.

Finally, the last line along which D'' switches its sign (and diverges) is the horizontal $g_x = 2Y^2$ passing through the sector vertex (cf. the denominator of eq 17).

Summarizing the above, there is an odd number of boundaries (specifically three) passing through each vertex and causing a change in polarity of D'', but never entering the interior of the sectors; the net effect thus should be a switch in polarity when crossing the vertex from one sector into another. A fast way to determine the signs of D'' is to check the limiting behavior of eq 17. For instance, for case 0 the limit of D'' for $g_x \to \pm\infty$ is negative, implying elliptic behavior in the lower sector and in the upper portion of the upper sector, with a hyperbolic region in between (cf. Figure 5). In the case 1 limit, say, for $\Delta g \to -\infty$ and $g_x \to -\infty$, with $|\Delta g| > |g_x|$, each of the four factors of eq 17 becomes negative (i.e., the numerator and denominator of the fraction, the criterion $\mathcal{H}$ of eq 19b, and the multiplier ρ_2 because of the transformation rules), leaving the overall sign of D'' again negative and the as-

signment elliptic. Note that it would be erroneous to view the sign of the boundary function $\mathcal{H}$ alone as the determining factor; in the above two examples it is positive and negative, respectively, yet in both cases it leads to the same elliptic type.

The same general pattern thus results for all three cases: (meta)stable elliptic behavior in the lower sector, switching to the (meta)stable hyperbolic one as the vertex is crossed into the upper sector, with one more elliptic region, this time, however, unstable, beyond the $\mathcal{H} = 0$ boundary. Note that while the width of the hyperbolic region does not converge to zero for $|\Delta g| \to \infty$ (since the sector vertices are different from hyperbola centers), its relative importance becomes negligible since the width of the neighboring unstable elliptic region grows without limits. The above assignments have been confirmed by numerical calculations.

4. Discussion

As demonstrated earlier, a HODCP has to be located on one of the three linear segments stretching in the triangular composition diagram between the three binary critical points (Figure 3). In addition to this compositional restriction, also the interaction parameters Δg and g_x are required to be within certain range of values (Table I), and the mean solvent interaction parameter $\bar{g}$ has to assume the value fixed by eq 15.

Specifically, a HODCP located on segment 0 (Figure 5) requires that

$$|g_x - 2\mu^2| > |\Delta g + 2\mu(1 + \nu)| \tag{21}$$

where μ and ν are defined by eq 14. A hyperbolic HODCP is produced if also

$$g_x[g_x - 2(\mu^2 + \nu^2 + \nu)] < \Delta g[\Delta g + 2\mu(1 + 2\nu)]$$

and

$$g_x > 2\mu^2 \tag{22}$$

while in the remaining instances the HODCP is of elliptic type, either stable (if $g_x < 2\mu^2$) or unstable.

For HODCP's case 1 (Figure 6) it is demanded that

$$|g_x - 2\nu^2| < |\Delta g + 2\nu(1 + \mu)| \tag{23}$$

with the additional condition of both arguments in eq 23 having the same sign. Hyperbolic types result if also

$$g_x[g_x - 2(\nu^2 + \mu^2 + \mu)] > \Delta g[\Delta g + 2\nu(1 + 2\mu)]$$

and

$$\Delta g > -2\nu(1 + \mu) \tag{24}$$

otherwise, the HODCP is of elliptic type, stable (if $g_x < 2\nu^2$) or unstable. For the case 2 (Figure 7) not only the signs of μ and ν in eq 23 and 24 are switched (cf. Table I) but also the orientation of the definition range changes. In the criterion

$$|g_x - 2\nu^2| < |\Delta g - 2\nu(1 - \mu)| \tag{25}$$

the two arguments are now required to be of opposite sign, and the additional condition for hyperbolic types becomes

$$g_x[g_x - 2(\nu^2 + \mu^2 - \mu)] > \Delta g[\Delta g - 2\nu(1 - 2\mu)]$$

where

$$\Delta g < 2\nu(1 - \mu) \tag{26}$$

The stability criterion for elliptic HODCP's stays the same as in case 1.

4.1. Vertex Systems and Their Neighborhood. The exclusive status of each vertex V as the origin of relative interaction coordinates $g^\dagger$ permitting the construction of a universal function for the mean solvent interaction parameter $\bar{g}^\dagger$ at a HODCP (cf. eq 15c) is also reflected in a unique physical behavior of such mixtures. Although at $g_x = g_x^v$ the parameter $\bar{g}$ in general diverges, at the vertex the ill-behaving last term of eq 15a becomes of 0/0 indeterminate type with a zero limit in all but one direction; thus $\bar{g}$ is well defined there (eq 15b). The positional indeterminacy of the HODCP whose w_2 also becomes of 0/0 type may seem to be disturbing at first sight (cf. eq 10). Yet, the situation is physically sound: each vertex represents a very special system whose critical line $T(w_2)$ (or one of its portions) is horizontal, running linearly between the two respective binary critical points.

Analogous behavior obviously occurs in a degenerate ternary system with two polymeric components identical in terms of *both* chemical nature *and* chain length. In fact, this trivial instance turns out to be one of a continuous spectrum of possible vertex-0 systems: note that for $r_1 = r_2$ one has $\mu = 0$ (cf. eq 14), with the vertex V_0 indeed located at the origin $g_x = \Delta g = 0$ (cf. eq 13). Similarly, the vertex systems for the cases 1 and 2 can be related to a common even more trivial "proto-system" of a "solution of monomers", $r_1 = r_2 = 1$. Thus it may be concluded that each vertex V_k represents a delicately balanced system where the effect of unequal chain lengths r_i and r_j on the critical temperature is just neutralized by combination of the interaction parameter g_{ij} and the difference $g_{ik} - g_{jk}$ such as to keep the critical temperature independent of the relative amounts of components i and j in the mixture. It is quite remarkable that such a balancing act is possible over the entire composition range; the existence of such systems could hardly have been anticipated.

Some simple results predicted by our analysis can be rationalized by common-sense arguments. Readily understandable, for instance, are changes caused by simple perturbations of the above alluded to degenerate system with $r_1 = r_2$: Changing Δg while keeping $g_x = 0$ (left–right displacement from the vertex in the diagram analogous to that of Figure 5) should result in a difference in critical temperatures of polymers 1 and 2 with the solvent, leading to a critical line which is primarily *sloped* but otherwise linear, i.e., with no HODCP. On the other hand, changing only the polymer–polymer interaction g_x has to yield a critical line whose two ends stay fixed at the same temperature (since $\Delta g = 0$) but which develops an *extremum* (i.e., a HODCP) because of attractions or repulsions between the unlike polymer segments. Hence, this vertical perturbation has to take the system into the HODCP definition range—as indeed confirmed by quantitative analysis. Similarly, one can justify the shift of the vertex into negative Δg range with growing difference between r_2 and r_1 purely by binary considerations where for the critical state with solvent, $r_2 > r_1$ clearly implies that $g_2 < g_1$, i.e., $\Delta g < 0$.

Elaborating on the above example with an extremum, one could even make a case for the assignment of hyperbolic and elliptic types to the positive- and negative-g_x neighborhood of the vertex, respectively: For instance, a positive δg_x, expressing an increase in repulsive interactions between polymers 1 and 2, reduces the number of 1–2 contacts and increases all others, thereby improving the solubility of polymers 1 and 2 in the solvent 0. Thus the observed pattern should be a one-phase stable region at middle compositions w_2 (where the 1–2 contacts are most frequent), separating two two-phase (or critical) regions attached to the binary sides 0–1 and 0–2, i.e., a behavior typical of hyperbolic HODCP's (cf. Figure 2).

While it is gratifying that one can qualitatively anticipate the outcome in the above simple examples, it is ev-

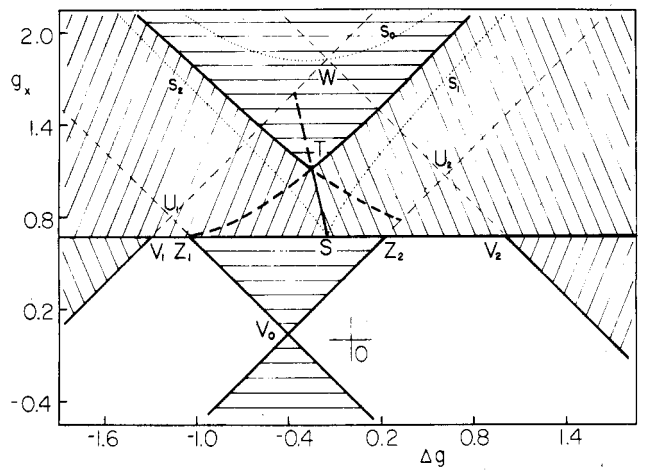

Figure 9. Bird's-eye view of the combined plot of Figures 5–7 displaying the overlap of the three HODCP surfaces around the sector vertices V_0, V_1, and V_2. Visibility is indicated by full-dashed pattern of curves of intersection and linear bounds of definition ranges and by the characteristic hatching of the top surface. (···) Boundaries s_i between hyperbolic and elliptic regions, all on visible portions of surfaces; T, system with three HODCP's; O, origin.

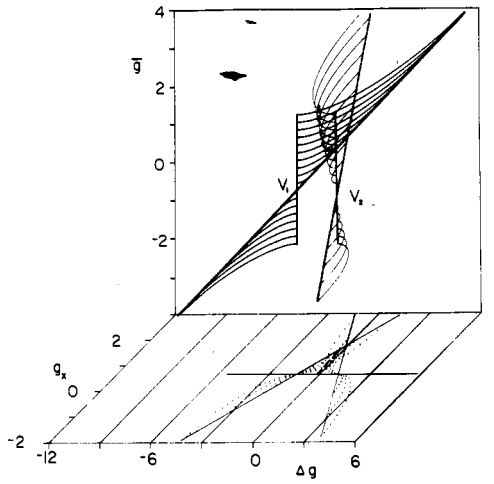

Figure 10. Three-dimensional view of surfaces 1 and 2 and their line of intersection (dashed). Notation is the same as in Figure 8, only the lines of constant $\bar{g}$ are incremented by 0.2.

ident that with macroscopic perturbations involving more than one independent variable the situation becomes too complicated for an intuitive insight, and one has to rely on the results of quantitative analysis. For instance, quite unexpected is the existence of the unstable elliptic region in the positive-g_x half-plane beyond the boundary s (Figures 5–7).

4.2. Multiple Occurrence of HODCP's in a System. The definition ranges displayed for the three cases separately in Figures 5–7 in fact partly overlap for $g_x > 2\nu^2$ as shown in Figure 9. The pattern of this overlap stays always the same, independent of chain lengths r_m:

(i) Because of the symmetrical bounds, the sectors 1 and 2 overlap in an isosceles triangle $\overline{V_1V_2WV_1}$ where the coordinates of W are $g_x = 2\nu(\nu + 1)$, $\Delta g = -2\mu\nu$, placing this point on the hyperbolic boundary of sector 0.

(ii) The relative positions of vertices V_k are always as depicted in Figure 9, satisfying the inequalities $0 \le g_{x,0}{}^v \le {}^1/_2$; $g_{x,0}{}^v \le g_{x,1}{}^v = g_{x,2}{}^v \le 2$; $-2 \le \Delta g_1{}^v \le \Delta g_0{}^v \le 0 \le \Delta g_2{}^v \le 2$. These and other facts guarantee overlaps of the sector 0 with sectors 1 and 2 in the form of two semiinfinite strips running diagonally up left and right (dashed lines in Figure 9), with the cut-away corner $\overline{Z_1V_0Z_2Z_1}$ and with the widths determined by the point W. On the other hand, the extensions of these strips in the opposite directions below the horizontal $\overline{V_1V_2}$ and below the lines $\overline{V_0Z_1}$ and $\overline{V_0Z_2}$, respectively, are entirely "empty", representing parameter combinations that cannot ever produce a HODCP. Typically the origin, $g_x = \Delta g = 0$, is located in the right empty region; only for a symmetrical system with $r_1 = r_2$ the origin overlaps with the vertex V_0.

(iii) Triple overlap occurs in the pentagonal region $\overline{Z_1Z_2U_2WU_1Z_1}$.

Physical significance of the overlap regions is in their signaling potential multiple occurrence of HODCP's. For a given system its interaction parameters are well-defined functions of temperature. This dependence can be plotted as a parametric curve in the g_x,Δg,$\bar{g}$ space, with temperature as the parameter; obviously such a curve—which might be called the system's trajectory in the space of interaction parameters—passes successively through all possible combinations of interaction parameters the given system can experience at various temperatures. If the interaction trajectory intersects a HODCP surface, the system will show at the respective temperature a double critical point. It is evident that a trajectory that happens to be in the proximity of an overlap region has a good chance to pass through more than one HODCP surface, with the corresponding system exhibiting at different temperatures two or more HODCP's located on two or more different segments.

In fact, some of the points in the overlap region share also the third coordinate—$\bar{g}$—giving rise to lines of intersection of two surfaces that represent loci of systems possessing two HODCP's at the same temperature. Equations of such curves are obtained by putting equal to each other $\bar{g}$'s of eq 15a for two different cases (surfaces). Thanks to the symmetry, particularly simple is the intersection of surfaces 1 and 2 that projects into the g_x,Δg base as a straight line,

$$g_x/\Delta g = -\nu/\mu \tag{27}$$

passing through the origin and through the common boundary point S ($\overline{ST}$ and its continuation in Figure 9). Since the slope is negative and its absolute value, ν/μ, is always greater than that of the boundary s_2 at the point S, $\nu/(\mu + \nu^2 - \mu^2)$, the line of intersection remains contained in the hyperbolic portions of both surfaces 1 and 2. Consequently, both of the simultaneously appearing HODCP's have to be of hyperbolic (meta)stable type; no elliptic type is allowed. A three-dimensional view of the intersecting surfaces 1 and 2 is shown in Figure 10.

The intersections of the surface 0 with surfaces 1 and 2 project into the g_x,Δg base as hyperbolas whose focal axes deviate from the vertical by an angle of $\pm{}^1/_2 \arctan[(1 + z)^{-1}]$; their equation is

$$z\Delta g^2 - (2 + z)g_x{}^2 \pm 2\Delta g g_x + 4\mu\nu(1 + z)\Delta g + 2[z \pm 2\mu\nu + (z + 2)(\mu^2 + \nu^2)]g_x = 0 \tag{28}$$

with the top signs and $z \equiv \nu + \mu$ characterizing the surface 1 intersection and the bottom signs and $z \equiv \nu - \mu$ standing for the surface 2 intersection. The lower physically unimportant branches of both hyperbolas pass through the origin and through the vertex 0 (not shown in Figure 9) but never enter the definition ranges of their surfaces. The upper branches, on the other hand, pass through the vertices of their respective surfaces with zero (horizontal) slope $dg_x/d\Delta g$, and are in part physically significant (bold in Figure 9). An analysis of their asymptotes shows that, just as before in the 1×2 case, the lines stay within hyperbolic regions of the involved surfaces. Thus, no elliptic

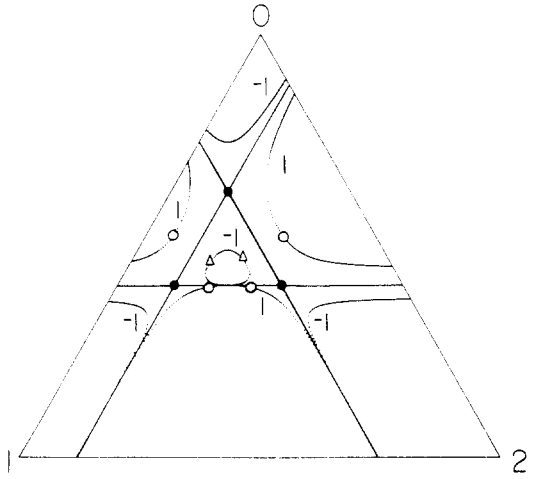

Figure 11. System with three hyperbolic HODCP's (●) and three linear spinodals at T_0 (for $r_1 = 2$ and $r_2 = 5$, eq 29 defines $g_x = 1.1193$, $\Delta g = -0.2520$, and $\bar{g} = 1.5293$). Spinodals for T_1 and T_{-1} have been obtained with $\bar{g} = 1.42$ and $\bar{g} = 1.63$, respectively, while keeping g_x and Δg unchanged. Single critical points: (○) (meta)stable; (△) unstable.

HODCP can ever coexist at the same temperature with another HODCP.

The three lines of intersection cross at the point T common to all three surfaces, physically corresponding to the only combination of interaction parameters that leads to the simultaneous occurrence of three HODCP's at the same temperature. It is given by the relations

$$g_x = 2\nu^2\tau \qquad \Delta g = -2\mu\nu\tau \qquad \bar{g} = \nu(\nu + 1)\tau \tag{29}$$

where $\tau = 1 + [\rho_1\rho_2/(1 + \rho_1 + \rho_2)]$ is a factor greater than one specifying the distance between the origin and point T in the base-plane projection, $\overline{OT}$, relative to that between the origin and the point S, $\overline{OS}$ (cf. Figure 9). It can be proven that the point T is always physically significant (i.e., it stays within the definition range of all three surfaces). In a system with interaction parameters given by eq 29, the six spinodal branches degenerate into three straight lines parallel to the composition triangle sides with equations

$$\varphi_0 = \frac{\rho_1\rho_2}{(1 + \rho_1)(1 + \rho_2)} \qquad \varphi_1 = \frac{\rho_2}{(1 + \rho_1)(\rho_1 + \rho_2)} \qquad \varphi_2 = \frac{\rho_1}{(1 + \rho_2)(\rho_1 + \rho_2)} \tag{30}$$

The three hyperbolic HODCP's are located at the intersections of the three spinodal lines (see Figure 11). For the mixture of monomers, $r_1 = r_2 = 1$, eq 30 yields the known symmetrical result $\varphi_0 = \varphi_1 = \varphi_2 = {}^1/_4$.[3]

The three-dimensional aspect of the overlapping region is emphasized in the bird's-eye view of Figure 9 where the visibility of the bold intersection lines is indicated by the full/dashed pattern, and the top surface (with maximal $\bar{g}$) is identified by its characteristic hatching. Thus, e.g., at the point W the mean solvent parameters of the three surfaces follow the sequence $(\bar{g})_0 > (\bar{g})_1 > (\bar{g})_2$, at U_1 it is $(\bar{g})_2 > (\bar{g})_0 > (\bar{g})_1$, and at U_2 one finds $(\bar{g})_1 > (\bar{g})_0 > (\bar{g})_2$. It should be noted that a large part of the visible top surfaces in the upper portion of the graph is thermodynamically not stable; in geographical terms this includes surface 0 north of s_0, surface 1 southeast of s_1, and surface 2 southwest of s_2.

4.3. Behavior in the Proximity of a (Meta)stable HODCP Surface. The sequence of events occurring around the HODCP temperature (Figures 1 and 2) is caused by the representative point moving on the system's trajectory in the 3-D space of interaction parameters and crossing the HODCP surface. An interesting question is, can one tie the polarity of the outcome to the direction of crossing? For instance, under normal circumstances (i.e., in the stable region) one might intuitively expect the space *above* the $\bar{g}$ surface to be associated with a solvent power inferior to that of the space *below* the surface. If so, an "upward" crossing should lead to the *formation* of real closed-loop binodals and spinodals for an elliptic HODCP (sequence T_0, T_1, T_2, T_3 in Figure 1) and to the *disappearance* of real critical points in the case of a hyperbolic HODCP (sequence T_2, T_1, T_0, T_{-1} in Figure 2). Consequently, the pairs of real critical points arising by splitting of a HODCP should exist only *above* the surface in elliptic regions but *below* the surface in the hyperbolic portions. Specifically for a system with a trajectory intersecting the HODCP surface vertically ($\delta g_x = \delta\Delta g = 0$) this would imply that an elliptic HODCP should be associated with a *minimum* of the critical line $\bar{g}(w_2)$, while a hyperbolic type should be situated at its *maximum*.

The above statements can be proven correct by examining the second derivative of the critical line, $\bar{g}'' \equiv d^2\bar{g}/dw_2^2$, for such a system. In order to reduce the number of independent variables, φ can be expressed explicitly from the G_c function, eq 2, and substituted into eq 1 and 3. Thus modified function F_c then directly yields the total derivative $d\xi^2/dw_2$ at a HODCP, characterizing how fast the critical line $\xi^2(w_2)$ embedded within the ξ^2 surface swings from one of its portions across the "weld" onto another portion. The result can be simplified in terms of previously introduced quantities as

$$\frac{d\xi^2}{dw_2} = -\frac{\mathcal{D}^2}{r_1r_2^2\mathcal{H}} \tag{31}$$

where $\mathcal{D}$ is the denominator of eq 10, and $\mathcal{H}$ is the boundary function of eq 19b. Four points related to eq 31 are worth mentioning: (i) At a vertex ($\mathcal{D} = 0$) this derivative becomes zero, consistently with our above interpretation of the vertex systems. (ii) At the hyperbolic/elliptic boundary s ($\mathcal{H} = 0$) the derivative diverges, implying a critical line $\xi^2(w_2)$ that crosses the "weld" perpendicularly and forms in the composition-triangle projection a cusp touching the linear segment (like the HODCP located on segment 0 in Figure 3). (iii) For HODCP's residing on the solvent segment 0 the derivative 31 is negative for elliptic types and positive for hyperbolic ones. For HODCP's located on polymer segments 1 or 2 the sign assignments are reversed. (iv) Equation 31 and the statements (i)–(iii) are not limited by the condition $\delta g_x = \delta\Delta g = 0$ but they are generally valid.

With the aid of eq 31, the above sought second derivative $\bar{g}''$ for a system with invariant g_x and Δg can now be obtained from the function H_c (eq 3). For the case 0 the result is

$$\bar{g}'' = \frac{D^4}{4(\rho_1\rho_2)^7(g_x^{\dagger})^2\mathcal{H}}\left(1 + \frac{w_1r_1 + w_2r_2}{w_1\rho_1 + w_2\rho_2}\right) \tag{32}$$

For cases 1 and 2 the signs of ρ are modified as usual (cf. Table I). The term in parenthesis is always positive, leaving just $\mathcal{H}$ and ρ_m to possibly affect the sign of $\bar{g}''$. Detailed consideration of signs of these two quantities for various instances indeed confirms that the statement formulated above is correct: e.g., a hyperbolic HODCP on segment 1 ($\rho_1 > 0$, $\rho_2 < 0$, $\mathcal{H} > 0$) is characterized by $\bar{g}'' < 0$, with the critical line $\bar{g}(w_2)$ displaying a maximum.

For a general system with other than a vertical trajectory the criterion can be derived from the $\bar{g}$-surface equation

Table II
Signs of Interaction Parameter Perturbations Improving the Solvent Power at Various HODCP's

case[a]	w_2	$(1 - \mathcal{G}^2)^b$	$\mathcal{G}^b$	$\delta\bar{g}$	δg_x	$\delta\Delta g$
0	$<w_2^S$	+	+	−	+	+
0	$>w_2^S$	+	−	−	+	−
1	$<w_2^S$	−	+	−	−	+
2	$>w_2^S$	−	−	−	−	−

[a] See Table I. [b] The signs of coefficients in relation 33b.

(15a), in the form of a universal function of the vertex-related quantity

$$\mathcal{G} \equiv \Delta g^\dagger / g_x^\dagger = (w_1\rho_1 - w_2\rho_2)/(w_1\rho_1 + w_2\rho_2) \quad (33a)$$

where the transcription in terms of ρ_m's holds again for case 0 and is subject to transformation for cases 1 and 2 (cf. Table I). For instance, all perturbations of a HODCP system such that

$$\delta\bar{g} > [(1 - \mathcal{G}^2)\delta g_x + 2\mathcal{G}\delta\Delta g]/4 \quad (33b)$$

will shift the system *above* the HODCP surface where the solvent power for the polymer mixture is diminished, with all the consequences following (development of closed-loop binodals around elliptic types, etc.). Conversely, interaction parameter variations that do not satisfy relation 33b place the system's representative point *below* the $\bar{g}$ surface where the solubility is improved. As might have been anticipated, the outcome does not depend only on the sign of $\delta\bar{g}$ alone, but also on $\delta\Delta g$ and δg_x.

Besides providing a quantitative criterion, eq 33b offers some qualitative guidance. For instance, for a HODCP located on the solvent segment 0 at $w_2 > w_2^S$ (where $-1 < \mathcal{G} < 0$), the solubility tends to improve by (i) a decrease in $\bar{g}$, (ii) an increase in g_x, and (iii) a decrease in Δg. The results for this and other cases are summarized in Table II. The mean solvent parameter $\bar{g}$ is seen to be the only one that shows a consistent effect on solubility under all circumstances; however, it should be kept in mind that its effect can be overshadowed by changes in other interactions.

Interpreting condition 33b in terms of temperature changes for a particular system requires replacing the variations of g's by their temperature derivatives. If such a modified condition is satisfied, the solubility will improve by a decrease in temperature. If, on the other hand, the inequality does not hold, the solvent power should increase as the temperature is raised. For instance, for the commonly assumed form $g = \alpha + \beta/T$, the solubility increases with growing temperature if

$$\bar{\beta} > [(1 - \mathcal{G}^2)\beta_x + 2\mathcal{G}\Delta\beta]/4 \quad (34)$$

In conclusion it is noted that the term "solvent power" used in this section should be understood strictly locally for the immediate neighborhood of the HODCP. It is realized that in ternary and higher systems the solubility (judged by the extent of two-phase regions) may simultaneously improve in one composition region while deteriorating in another.

4.4. Orientation of Spinodals at HODCP's. Often it is desirable to have some knowledge about the direction of the spinodal at the critical point. Normally its slope can be obtained as a limit of tie-line slopes;[6] with ξ^2 of eq 5 the formal result for a HODCP residing on segment 0 is

$$[d\varphi_2/d\varphi_1]_c = w_2\rho_2/(w_1\rho_1) \quad (35)$$

For other instances the signs of ρ's are modified as usual (cf. Table I). However, in the case of HODCP's the interpretation of this formula calls for closer attention. For the elliptic type the spinodal has degenerated to an infinitesimal size, and the slope of eq 35 can be viewed only as the limit of critical spinodal directions as the closed-loop curves shrink in size to become a HODCP. In other words, it defines a direction conjugate to the limiting diameter connecting the pairs of critical points on the opposite sides of incipient spinodal loops.

While in the hyperbolic case the above interpretation is still in principle valid, one would much rather have the directions of the two asymptotes into which the spinodals degenerate at a HODCP. These can be evaluated from the solved quadratic spinodal equation (8); after some simplification one gets

$$(d\varphi_2/d\varphi_1)_{as} = [-2U \pm (2D'')^{1/2}]/(4A_0) \quad (36)$$

where D'' is given by eq 17. For the case 0, U and the limit of A of eq 8 take the form

$$U = \rho_1\rho_2(\mathcal{G}^2 - 1)g_x^\dagger + 2(1 + \rho_1)(1 + \rho_2) \quad (37)$$

$$A_0 \equiv \lim_{\substack{D\to 0 \\ D'\to 0}} A = \rho_1\rho_2[\tfrac{1}{2}(\mathcal{G}^2 - 1) - (\mathcal{G} + 1)\rho_2]g_x^\dagger + (1 + \rho_2)^2 \quad (38)$$

where, as before (eq 33a), $\mathcal{G}$ specifies the reciprocal slope of the radius vector in vertex-related coordinates $g_x^\dagger, \Delta g^\dagger$, also fixing w_2. The other two cases follow by switching signs of ρ_m as instructed in Table I.

Formula 36 indicates that the two asymptotes overlap only if $D'' = 0$, i.e., at the boundaries between elliptic and hyperbolic regions. This is understandable: the transition from a hyperbolic pattern with convex shapes relative to its center to an elliptic pattern with concave curvature has to go through a linear degenerate state where both curves (and the hyperbola's asymptotes) flatten to a single line. The orientation of this line, however, as well as the spinodal and stability patterns, is very different for the two instances where this situation can occur:

(i) The behavior is "normal" in vertex systems which are embedded in stable regions. Thanks to the condition $g_x^\dagger = 0$, eq 36 is simplified; e.g., for the case 0 one gets

$$(d\varphi_2/d\varphi_1)_{as}^V = -(1 + \rho_1)/(1 + \rho_2) \quad (39)$$

which is recognized as the slope of the solvent segment 0. Thus the double spinodal asymptote overlaps with the corresponding linear segment, in conformity with conclusions of Section 4.1., and a small perturbation up or down in the $g_x, \Delta g$ plane generates the simplest posible hyperbolic or elliptic two-phase patterns, aligned with the critical line stretching between the two binary critical points (see Figure 12). The stability situation here is trivial; e.g., the inside phase of the loop-shaped spinodals in Figure 12b is unstable while the outside phase is (meta)stable.

(ii) D'' also equals zero at the hyperbolic boundaries s separating the elliptic and hyperbolic HODCP regions in the upper sectors of Figures 5–7, hence all such systems will again have the two asymptotes merged into one. Here, however, the double asymptote is no longer aligned with the segment but, from eq 19b and 36–38, its slope is

$$(d\varphi_2/d\varphi_1)_{as}^s = (1 - \mathcal{G})/(1 + \mathcal{G}) \quad (40)$$

Its direction varies continuously with changing w_2 between those of the adjacent triangle sides; e.g., for a HODCP located on segment 0, with w_2 varying from 0 to w_2^S to 1, $\mathcal{G}$ changes from +1 to 0 to −1, the slope goes from 0 to +1 to ∞, and the direction rotates from that of the 0–1 side to a vertical to that of the 0–2 side. Also the appearance of spinodals is very different from case (i). With D, D', and D'' all equal to zero but $D''' \neq 0$, the spinodal dis-

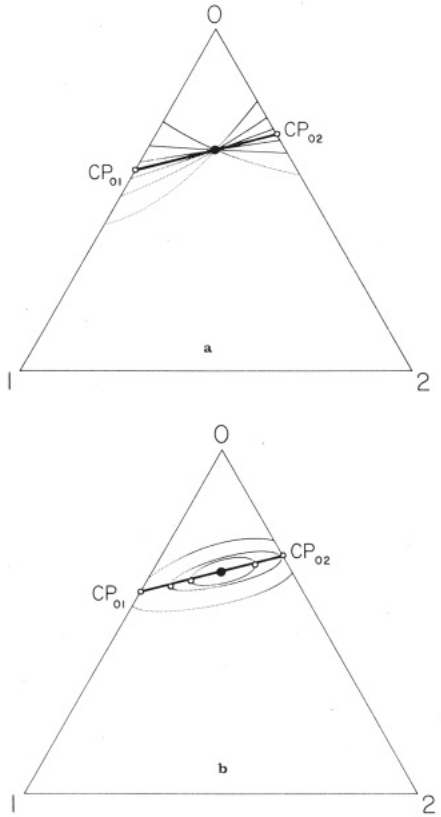

Figure 12. Deformation of hyperbolic and elliptic spinodals into a line $r_1 = 2$, $r_2 = 5$, case-0 systems approaching the vertex. (—) Linear spinodal for the vertex system ($\Delta g = -0.410$). (a) Spinodal asymptotes for three systems with hyperbolic HODCP's fixed at $w_2 = 0.5$; from outside in, Δg values are −0.450, −0.430, and −0.412. (b) Spinodals for three slightly perturbed elliptic-HODCP systems with $w_2 = 0.5$; from inside out, Δg is −0.380, −0.396, −0.408, and the perturbations $\delta\bar{g}$ of the HODCP values are 0.5%, 0.7%, and 1%, respectively.

criminant D versus φ_1 plot exhibits a point of inflexion with a horizontal slope, making the spinodal real only on one side of the HODCP. Consequently, the spinodal has to form a *cusp* just touching on the corresponding linear segment. The direction of approach can be decided from the sign of the discriminant's third composition derivative given for the case 0 and 2 by

$$D''' = -48\rho_1^4\rho_2^3[Y\Delta g + (X + 1)g_x]^2(g_x - \Delta g)/g_x^\dagger \qquad (41)$$

(The sign switches to positive for the case 1 because of the ρ_2 term.) Since $D''' < 0$ ($D''' > 0$) for case 0 and 2 (case 1), the discriminant is a descending (ascending) function of φ_1. This information, combined with the limited interval of asymptote orientations allowed by eq 40, leads to the conclusion that the spinodal cusps have to touch the triangle of linear segments 0, 1, and 2 from the *outside* (while it is recalled that the critical-line cusp touches it from *inside* as shown in Figure 3, segment 0). The nature of this puzzling structure can be clarified by inspecting the spinodal surface for three systems around the boundary s. The sketches shown in Figure 13 are based in part on analytical results given above, in part on numerical computations; they are plotted onto the composition base with $\bar{g}$ as the vertical.

(a) Formula 32 for the curvature of the critical line is not affected by stability considerations; thus even in the unstable region *beyond* the boundary s an elliptic HODCP appears as a minimum E of the critical line $\bar{g}(w_2)$ (and of the spinodal surface) for the respective system, with another established spinodal "ridge" somewhere in the neighborhood (Figure 13a). Note, however, that the stabilities of regions are switched: Normally (Figures 1 and 12b) the system is (meta)stable ouside the loops and unstable inside. In Figure 13a, on the other hand, the situation is reversed, and the critical points turn out to be unstable in Korteweg's sense.[1] Not surprisingly, the inside of the "ridge" is found to be (meta)stable just as the inside of the loops was.

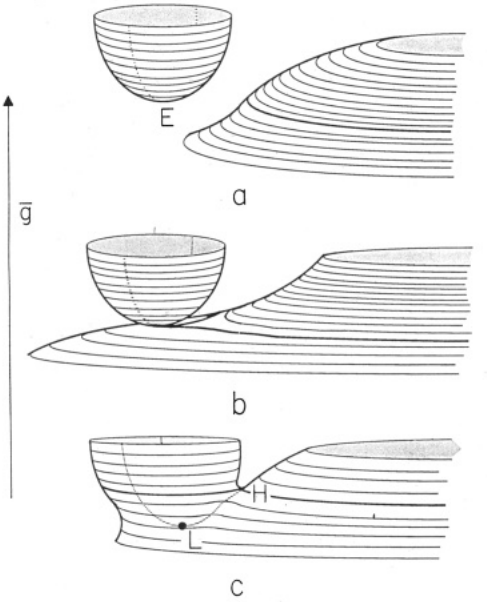

Figure 13. Schematic drawing of the spinodal surface $\bar{g}(w_2,\varphi)$ for three HODCP systems in the neighborhood of the boundary s. E, Unstable elliptic HODCP; H, (meta)stable hyperbolic HODCP; L, heterogeneous double critical point; (···) critical line $\bar{g}(w_2)$; bold line, spinodal corresponding to the HODCP temperature; shaded inside areas, (meta)stable phase; outside areas, unstable phase. The system is located (a) *beyond* the s boundary; (b) *on* the s boundary; and (c) *in front of* the s boundary.

(b) As the system's representative point in the $g_x,\Delta g$ space approaches the boundary s, the minimum surface is descending toward the "ridge" and both surfaces are becoming deformed. For a *boundary* system, the two surfaces form a contact which has essentially one-dimensional structure: The bottom spinodals of the minimum surface become infinitely asymmetric as they shrink to zero size, and their counterparts on the "ridge" are deformed into a cusp (Figure 13b). And, clearly, it is the direction of this aligned structure that is defined by eq 40. The opposite approaches of spinodal and critical line to the HODCP are seen to be the result of each curve originating in a different surface: the former one is part of the established "ridge", while the latter one is embedded in the minimum surface.

(c) For a system *in front* of the boundary s, the minimum spinodal surface has penetrated into the "ridge", forming a saddle point harboring the hyperbolic HODCP (Figure 13c). Three types of spinodals exist here: Closed-loop isotherms present at higher $\bar{g}$ become pointed and move to main spinodals as $\bar{g}$ is decreased. At the HODCP both portions join, forming a hyperbolic-asymptote pattern with two of its branches connected by a loop (bold in the sketch). Further drop in $\bar{g}$ swells the point-size neck into a bottleneck and, eventually, the residue of the original closed-loop spinodals is absorbed in the main-spinodal surface. The critical line, first only on the minimum surface (Figures 13a,b), now also crosses the saddle and forms two minima L (only one is visible) that have been shown to be heterogeneous double critical points. As always, they separate unstable critical points (left of L in Figure 13c) from (meta)stable critical points (right of L).

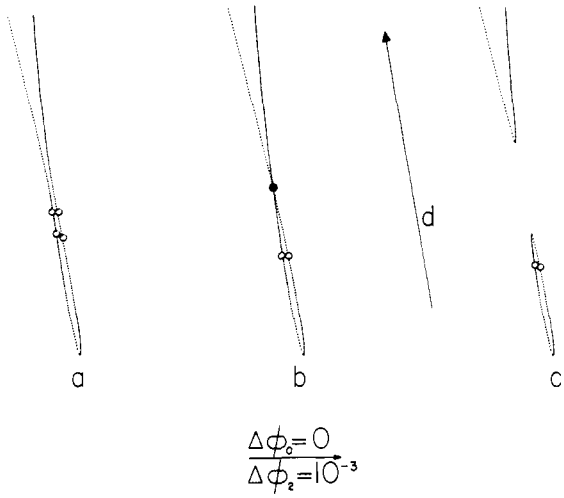

Figure 14. Three spinodal isotherms computed for the system $r_1 = 2$, $r_2 = 5$, case 0, with a hyperbolic HODCP similar to that of Figure 13c. Curves would normally overlap; here they are shifted for better clarity. Arrow *d* indicates the double-asymptote direction $d\varphi_2/d\varphi_1 = 1.948$ of eq 40; (●) HODCP; (○) single critical points. $\bar{g}$ values are (a) bottleneck 1.824 599, (b) HODCP 1.824 600 2, and (c) closed loop 1.824 602.

In this context it becomes apparent why the *s*-boundary systems have to also satisfy the criterion for heterogeneous double critical points: they represent the limiting case where the two minima *L* have just merged with the HODCP (saddle point).

The above outline is documented by a drawn-to-scale plot of three spinodals computed for an off-boundary system with a hyperbolic HODCP (Figure 14). The curves correspond to slices of the surface of Figure 13c taken at progressively higher values of $\bar{g}$ at constant $g_x = 2.108\,95$ and $\Delta g = -1.0772$. The orientation of spinodals is very close to the unique direction *d* predicted for the double asymptote at the HODCP for a boundary system.

5. Conclusions

Recently developed novel analysis of ternary systems has led to a host of new quantitative relations for homogeneous double critical points (HODCP's). Their position in the triangle of composition is restricted to three linear segments linking the three binary critical points (cf. Figure 3) and can thus serve as a means of distinction. The advantage of such classification into three groups (with labels 0, 1, and 2 specifying the triangle apex which is spanned by the segment) is that complicated general expressions become greatly simplified when applied specifically to a group of HODCP's residing on a particular segment.

A global diagram of all HODCP's that can exist on a given segment for a given set of chain lengths r_m is best plotted in the space of "heterointeraction" parameters g_x and Δg that express deviations of the examined system from the reference quasi-binary system (where $g_x = \Delta g = 0$). It appears that at a HODCP these interactions cannot be arbitrary; rather their permitted values are limited to a double-sector-shaped area that fans across a 90° (or 45°) interval of the g_x,Δg space, with the vertex position depending on chain lengths r_1 and r_2 (cf. Figures 5–7). The pair of coordinates g_x and Δg are the only variables free to choose; all other quantities (mixed-polymer composition w_2, total polymer volume fraction φ, and the mean polymer–solvent interaction parameter $\bar{g}$) are fixed by the HODCP conditions.

Sector vertices represent very special situations: e.g., in the vertex-0 system the effect of difference in chain lengths r_1 and r_2 on the critical temperature *T* is just compensated by interactions g_x and Δg so as to make *T* independent of the composition w_2 of the mixture of polymers 1 and 2. The critical line $T(w_2)$ of such systems is horizontal, running linearly between the respective binary critical points.

Distinction between the *elliptic* and *hyperbolic* HODCP's, marking the disappearance of closed-loop spinodals (Figure 1) and the confluence of two regular spinodal regions into a single one (Figure 2), respectively, can be made from the sign of the second composition derivative of the discriminant of the spinodal quadratic equation. Qualitatively, the result is the same for all three groups of HODCP's. Lower definition sectors in the g_x,Δg space contain exclusively elliptic types, while the upper sectors are split between hyperbolic (region adjacent to the vertex) and elliptic HODCP's (beyond the $\mathcal{H} = 0$ boundary), with the latter points being thermodynamically unstable. Hence, in addition to φ, w_2, and $\bar{g}$, also the type of a HODCP and its stability are uniquely determined by the interactions g_x and Δg.

Wherever the elliptic region meets the hyperbolic one, both types of spinodals degenerate in the neighborhood of the HODCP into essentially 1-D structures with a specific direction. This situation arises in two instances: (1) For systems around the vertex where the deformed spinodals become aligned with the linear segment connecting the two binary critical points (Figure 12). (2) At the hyperbola-shaped $\mathcal{H} = 0$ boundary in the upper sector where the spinodal develops a cusp, eventually leading to some exotic shapes as it exudes a "droplet", forms a bottleneck, etc. (cf. Figures 13 and 14), with the orientation being a function of polymer mixture composition w_2.

In the space of three interaction parameters $\bar{g}$, Δg, and g_x, the locus of each group of HODCP's is a section of a deformed double-cone surface (Figures 8 and 10). In a way, the sections are complementary: when plotted in relative, vertex-related coordinates they produce a smooth double half-cone. The development of spinodals around the stable region of this surface follows an intuitive expectation: an "upward" perturbation pointing above the surface (toward higher values of $\bar{g}$) deteriorates the solvent power, bringing forth the pattern −1 of Figure 2 for hyperbolic HODCP's and closed-loop curves for elliptic ones (1, 2, and 3 in Figure 1). Opposite behavior, i.e., an improvement in solubility, is observed for a "downward" displacement taking the system's representative point below the surface.

Three ranges of existence for the three groups of HODCP's partly overlap in the positive-g_x area. If the system's trajectory in the space of interaction parameters lies nearby, there is a good chance that the system will show two or more HODCP's located on different segments at different temperatures. Actually, the three surfaces intersect, forming three lines of intersection, and one point of intersection common to all three of them (Figure 9). Corresponding systems possess two or three HODCP's of hyperbolic type occurring simultaneously at one temperature; in the very special latter case the spinodals degenerate into three lines parallel to the sides of the composition triangle (cf. Figure 11).

Acknowledgment. Support by the National Science Foundation, Division of Materials Research, Polymers Program, Grant DMR-8511494, is gratefully acknowledged. We also thank M. Rozniak for technical help.

References and Notes

(1) Korteweg, D. J. *Arch. Néerl.* **1889**, *24*, 295.
(2) Šolc, K. *Macromolecules* **1987**, *20*, 2506.
(3) Meijering, J. L. *Philips Res. Rep.* **1950**, *5*, 333; **1951**, *6*, 183.

(4) Šolc, K. J. Polym. Sci., Polym. Phys. Ed. 1982, 20, 1947.
(5) Yang, Y. C.; Šolc, K. Polym. Prepr. (Am. Chem. Soc., Div. Polym. Chem.) 1987, 28 (2), 246.
(6) Šolc, K. Macromolecules 1986, 19, 1166.
(7) The term critical line as used in this report has a generic meaning of a locus of critical points in any coordinates. Traditional interpretation would be the critical temperature plotted as a function of critical composition for a given ternary system [coded as $T(w_2)$], but it could also be $\bar{g}(w_2)$ (since $\bar{g}$ is a well-defined function of temperature) or, e.g., $\xi^2(w_2)$ (where the critical value of ξ^2 is defined from eq 1-3). An attached qualifier speficies which critical line is concerned.
(8) See, e.g.: Šolc, K.; Koningsveld, R. J. Phys. Chem. 1985, 89, 2237.
(9) Šolc, K.; Kleintjens, L. A.; Koningsveld, R. Macromolecules 1984, 17, 573.
(10) Šolc, K.; Battjes, K. Macromolecules 1985, 18, 220.
(11) Scott, R. L. J. Chem. Phys. 1949, 17, 279.

Comparison of the Translational Diffusion of Large Spheres and High Molecular Weight Coils in Polymer Solutions

Wyn Brown* and Roger Rymdén

Institute of Physical Chemistry, University of Uppsala, Box 532, 751 21 Uppsala, Sweden.
Received May 19, 1987; Revised Manuscript Received September 12, 1987

ABSTRACT: The translational diffusion of large stearic acid coated silica spheres (R_H = 1595 Å) and high molecular weight polystyrene (PS) fractions in poly(methyl methacrylate) (PMMA) solutions has been examined by using dynamic light scattering (QELS) over the dilute/semidilute concentration ranges of the latter polymer. When the PMMA concentration is normalized by the overlap concentration, C^*, the reduced diffusion coefficient (D/D_0) for the sphere is a universal function of C_{PMMA}. A similar observation applies to the data for the PS fractions. This is in accord with scaling predictions. The product $D_{SiO_2}\eta$ is a constant, independent of both C_{PMMA} and M_{PMMA}, where η is the macroscopic solution viscosity of the medium. Thus the Stokes-Einstein equation applies. In contrast $D_{PS}\eta$ is an increasing function of C_{PMMA} and this trend is more pronounced at higher M_{PMMA}. Although the Stokes-Einstein mechanism is assumed to also apply with linear probe chains, it is concluded that there may be a significant coupling of the dynamics of the probe chain and those of the network polymer.

Introduction

Recently, considerable attention has been focused on the single-chain diffusion of a linear polymer in a matrix of a second polymer at semidilute concentrations. One approach has been to use dynamic light scattering (QELS) from isorefractive ternary solutions: the host polymer is index matched[1-13] to a simple solvent and the probe polymer (at very low concentration and having good optical contrast) studied as a function of molecular weight and matrix polymer concentration. This is the so-called "optical-labeling" technique where it is assumed[5] that QELS monitors self-diffusion at a low but finite concentration of the test chain. (It will differ from the more strictly considered self-diffusion coefficient of a spin-labeled individual in a sea of otherwise identical chains as determined, for example, in pulsed field gradient NMR, to the extent that there may be significant chemical and size differences between probe and host chains.)

Recent examples of the optical-labeling approach include use of polystyrenes (PS) as the probe chain in transient networks of poly(methyl methacrylate) (PMMA),[2,3,11,12] index matched with toluene or benzene, or poly(vinyl methyl ether) (PVME) in toluene[5,8] or *o*-fluorotoluene.[4,7,9,10] Chu and co-workers[13] have ingeniously included a second simple solvent so that the contrast can be also varied to match either the PS or PMMA.

For a recent discussion of such investigations one may refer to the paper of Numasawa et al.[11] From the accumulated data in the above studies, it is apparent that translational diffusion of a linear probe chain in the network of the second chain may proceed by two main processes.

1. **Stokes-Einstein (S-E) diffusion** which is governed by the macroscopic viscosity (η) of the host solution and the hydrodynamic radius (R_H) of the probe chain is given according to

$$D_s = kT/6\pi\eta R_H \quad (1)$$

Due to hydrodynamic screening effects, this process may become independent of the molecular weight of the guest chain and also exhibit extreme dependence on the concentration of the host polymer.

2. **Reptation** is the process whereby the probe chain diffuses along a fictive tube formed by the topological constraints of the surrounding chains. In a good solvent, this model leads to the scaling prediction:[14]

$$D_s \sim M^{-2}C^{-1.75} \quad (2)$$

Thus D_s should be strongly dependent on the chain length (guest polymer) and also the concentration (C) of the matrix polymer. D_s may also become independent of the molecular weight of the matrix polymer, however. Recent discussions have centered on modifying effects (the "noodle" effect[15] and constraint release[16,17]) which model contributions from surrounding chains, and these lead to modifications in the scaling expression.

Although the above remarks center on the results obtained in ternary systems, we note the possible presence in binary systems of translational motion motion in semidilute solutions.[20-23] Thus even in good solvents the photocount autocorrelation function may be bimodal[20,42,43] (gel mode accompanied by translation). As the solvent quality is reduced, toward Θ conditions an additional very slow mode becomes evident in the CONTIN inversion of the time correlation function and this may be attributed to a structural relaxation and/or motions of clusters of chains.[44-47] In the ternary systems the main processes (1 and 2 above) play different relative roles depending on the concentration of the matrix polymer as well as the relative sizes of host and matrix chains. S-E diffusion apparently extends throughout much of the usually defined semidilute region[5,8-11,48] up to the point where extensive interpene-

0024-9297/88/2221-0840$01.50/0